LANGMUIR

Article

pubs.acs.org/Langmuir

Time-Resolved Neutron Reflectivity during Supported Membrane Formation by Vesicle Fusion

Alexandros Koutsioubas,*[,†] Marie-Sousai Appavou,[†] and Didier Lairez[‡,§]

[†]Jülich Centre for Neutron Science (JCNS) at Heinz Maier-Leibnitz Zentrum (MLZ), Forschungszentrum Jülich GmbH, Lichtenbergstr. 1, 85748 Garching, Germany

[‡]Laboratoire des Solides Irradiés, École Polytechnique, CNRS, CEA, Université Paris-Saclay, 91128 Palaiseau cedex, France

[§]Laboratoire Léon Brillouin, CNRS, CEA, Université Paris-Saclay, 91191 Gif-sur-Yvette cedex, France

Supporting Information

ABSTRACT: The formation of supported lipid bilayers (SLB) on hydrophilic substrates through the method of unilamelar vesicle fusion is used routinely in a wide range of biophysical studies. In an effort to control and better understand the fusion process on the substrate, many experimental studies employing different techniques have been devoted to the elucidation of the fusion mechanism. In the present work, we follow the kinetics of membrane formation using time-resolved (TR) neutron reflectivity, focusing on the structural changes near the solid/liquid interface. A clear indication of stacked bilayer structure is observed during the intermediate phase of SLB formation. Adsorbed lipid mass decrease is also measured in the final stage of the process. We have found that it is essential for the analysis of the experimental results to treat the shape of adsorbed lipid vesicles on an attractive substrate theoretically. The overall findings are discussed in relation to proposed fusion mechanisms from the literature, and we argue that our observations favor a model involving enhanced adhesion of incoming vesicles on the edges of already-formed bilayer patches.

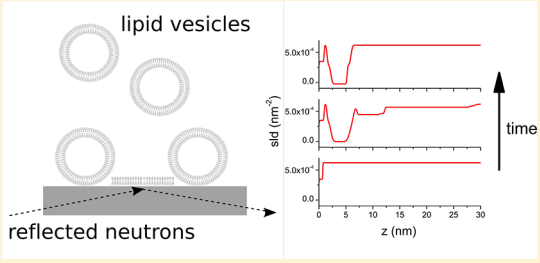

INTRODUCTION

Biophysical investigations relying on the use of supported lipid bilayers (SLB) are proving useful in the elucidation of model membrane structure and interaction with biological molecules. The special nature of SLB (i.e., their reconstitution on a planar surface and separation from it by a subnanometer water layer) enables the application of many different surface-sensitive experimental techniques, such as atomic force microscopy,[1] quartz crystal microbalance,[2,3] evanescent wave methods,[4] and neutron/X-ray reflectivity.[5,6]

The spreading (or fusion) of small (SUV) or large (LUV) unilamellar vesicles on hydrophilic surfaces, pioneered by McConnell el. al.,[7] provides a simple and versatile method for the preparation of SLBs. Owing to widespread interest, the mechanism of SLB formation via vesicle fusion has been studied by several groups, and the subject has been extensively reviewed.[3,8,9] The influence of many different factors affecting the propensity of vesicles to form high-quality SLBs has been investigated as the physicochemical properties of the supporting surface,[10] lipid head charge,[11] solution pH and ionic strength,[12] and vesicle size and composition.[1,13]

The general picture drawn from different studies concerning the steps involved in the formation of SLB via vesicle fusion includes an initial adsorption of intact vesicles on the substrate, subsequent rupture, and finally their spreading leading to coalescence and full coverage.[8] It is acknowledged that the attraction between lipid heads and the surface plays an important role, whereas the existence and nature of structural intermediates during the vesicle deposition process is a matter of ongoing research. The term "structural intermediate" refers to the shape and collective arrangement of vesicles prior to and during their spreading on the substrate. For example, it is not clear if the spreading proceeds via deformation and rupture of single vesicles[1] or if after reaching a certain coverage, the fusion of neighboring adsorbed vesicles is taking place prior to rupture.[2] In addition, other recent studies have reported additional phenomena such as the crucial role of active bilayer patch edges that catalyze membrane formation[14,15] and the desorption of lipid vesicles in the stage of SLB completion.[16]

Differences that appear in the literature between proposed fusion mechanisms are related to experimental limitations and also to the fact that each technique probes different physical properties. A large part of the relevant experimental information to date comes from ensemble techniques such as quartz crystal microbalance (QCM) and surface plasmon resonance (SPR) that have high time resolution, giving information about the adsorbed lipid mass and about the viscoelastic properties of the adsorbed layer (in the case of QMC with dissipation).[3] Real space techniques such as in situ atomic force microscopy (AFM) can give valuable insights on the single-vesicle scale but suffer from low time resolution, something that has recently been addressed using elaborate microscopy techniques.[17]

Received: July 14, 2017
Revised: August 16, 2017
Published: September 5, 2017

DOI: 10.1021/acs.langmuir.7b02459
Langmuir 2017, 33, 10598−10605

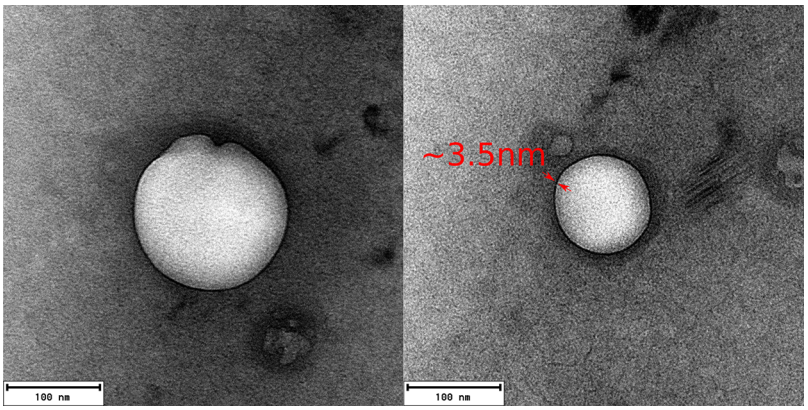

Figure 1. Typical cryo-transmission electron micrographs of the lipid vesicles.

However, microscopy even at high spatiotemporal resolution gives a "bird's eye" view of the system, where near-surface information on the nanometer scale is not accessible.

Neutron and X-ray reflectivity offer the possibility to obtain a detailed nanometer-scale picture of the molecular distribution at the solid−liquid interface and have been implemented in the past for the study of vesicle fusion.[5,6] Here we revisit the use of neutron reflectivity under a constant solution flow setup and low vesicle concentrations in order to capture the reflectivity of the system during the various stages of the SLB formation process. We choose to work with a system of zwitterionic phospholipids on a hydrophilic substrate that is most commonly used in studies that attempt to elucidate the vesicle spreading mechanism on a substrate. Additionally, the kinetics of this particular model system have been extensively studied, and it is well established that the formation kinetics scale with concentration down to the ng/mL concentration range, thus permitting the observation of the different phases of the phenomenon with techniques (such as neutron reflectivity) characterized by lower time resolution. Model fitting of the reflectivity curves acquired during the fusion of phospholipid LUV on SiO_2 provides interesting insights in relation to results from real-space techniques. In particular, our observations compare favorably with a recently proposed mechanism that considers membrane patch edges as high-affinity surfaces for vesicle adsorption.[14,15]

MATERIALS AND METHODS

Lipid 1-palmitoyl-2-oleoyl-*sn*-glycero-3-phosphocholine (POPC) was purchased from Avanti Polar Lipids in the form of lyophilized powder and was used without any further purification. Deuterium oxide (D_2O) of 99.8% purity was purchased from ARMAR (Europa) GmbH. Ultrapolished Si blocks (r.m.s. roughness of 0.2 nm, dimensions 150 × 50 × 20 mm^3) purchased from Andrea Holm GmbH were used as substrates and were cleaned as previously described.[18]

Unilamellar vesicles in D_2O buffer (150 mM NaCl, 5 mM HEPES, pD = 7.4) were prepared by sonication as described in a previous work.[18] The size of the LUVs was characterized by dynamic light scattering (DLS) using a Malvern Zetasizer Nano-S (Malvern Instruments Ltd., Malvern U.K.) at 25 °C. The acquired autocorrelation function was analyzed by cumulant analysis, based on nonlinear least-squares fits with Malvern's Zetasizer software v. 7.11 (International Standard ISO22412 Particle Size Analysis - Dynamic Light Scattering, International Organisation for Standardisation (ISO) 2008). It is a moment expansion that gives as the first two terms the *z*-average size (that represents the intensity-weighted mean hydrodynamic diameter) and the polydispersity index (PDI) that informs us about the distribution of vesicle size.

Samples for cryo-transmission electron microscopy (cryo-TEM) were prepared by placing a drop of the 0.5 mg/mL vesicle solution on a Quantifoil Multi A carbon-coated copper grid. After a few seconds, excess solution was removed by blotting with filter paper. This sample was cryo-fixed by rapid immersion into liquid ethane at −180 °C in a cryo-plunge (EMGP Leica GmbH). The specimen was inserted into a cryo-transfer holder (HTTC 910, Gatan, Munich, Germany) and transferred to a JEM 2200 FS EFTEM instrument (JEOL, Tokyo, Japan). Examinations were carried out at temperatures of around −180 °C. The transmission electron microscope was operated at an acceleration voltage of 200 kV. Zero-loss filtered images were taken under reduced dose conditions (<10 000 e^-/nm^2). All images were recorded digitally by a bottom-mounted 16 bit CCD camera system (TemCam-F216, TVIPS, Munich, Germany). To avoid any saturation of the gray values, all the measurements were made with intensity below 15 000. Images have been taken with an EMenu 4.0 image acquisition program (TVIPS, Munich, Germany) and processed with a free digital imaging processing system, ImageJ.[19]

Neutron reflectivity data were acquired at the MARIA vertical reflectometer[20] of the JCNS outstation at MLZ in Garching (Germany), using temperature-regulated (25 °C) custom liquid cells. The design of the liquid cells (volume ∼4 mL) is similar to that used in previous work.[21] An injection of vesicle solutions at a constant flow rate (1 mL/min) is performed by connecting the liquid cell inlet to a syringe pump (Pump 11 Elite, Harvard Apparatus). Measurements were performed using two different wavelengths (1 nm for the low-q region and 0.5 nm for the high-q region up to 2.5 $nm^{-1)}$, with a wavelength distribution fwhm of $\Delta\lambda/\lambda = 0.1$.

The acquired neutron specular reflectivity profiles were analyzed by classic model fitting using a custom simulated annealing minimization algorithm written in Fortran 90. Theoretical curves were calculated using the Abelès matrix formalism[18,22] where each layer n is defined by three parameters: the scattering-length density (sld) ρ_n, thickness d_n, and roughness σ_n. Phospholipid bilayers are represented by a three-layer stack corresponding to their lipid heads/tails−tails/heads structure, where the two lipid head layers are identical, and the relative sld of the head and tail layers is related through the molecular structure of POPC. The layer roughness is introduced by applying Névot-Croce correction terms to the Fresnel coefficients.[23]

Because a two-dimensional position-sensitive detector is used at a MARIA instrument for the measurement of the reflected beam, except from the specular component of the reflectivity (where the incident angle α_i is equal to the exit angle α_f), we also register the off-specular reflectivity ($\alpha_i \neq \alpha_f$) in which the scattering wavevector is not strictly perpendicular to the sample surface and thus possesses a component along q_x so that in-plane structures can be probed. In this case, the relation between reciprocal-space coordinates and the instrumental parameters is given by[24]

$$q_x = (2\pi/\lambda)(\cos\alpha_i - \cos\alpha_f) \quad (1)$$

DOI: 10.1021/acs.langmuir.7b02459
Langmuir 2017, 33, 10598−10605

$$q_z = (2\pi/\lambda)(\sin \alpha_i - \sin \alpha_f) \quad (2)$$

RESULTS

Vesicle Characterization. Vesicles prepared by sonication were characterized before reflectivity measurements by DLS and cryo-TEM. Analysis of the DLS data suggests an overall vesicle diameter (z average) equal to ∼104 nm with a PDI of about 0.2 and small variations of ±0.05 between different preparation runs.

Cryo-TEM images (Figure 1) of the samples gave us information about the overall morphology of the vesicles. An inspection of the cryo-TEM images revealed that for the vast majority of vesicles (>95%) there is no entrapment of smaller vesicles inside larger ones, i.e., no appreciable oligovesicular structures present. Additionally from the thickness of the high-contrast border that is visible at the vesicle extremities, we may estimate any residual oligolamellarity. In all analyzed pictures, the thickness of the high-contrast vesicle border was always equal to ∼3.5 nm, which is close to the typical value expected for a single phospholipid bilayer membrane.

Membrane Formation Kinetics. Taking into account that SLB formation scales with exposure (vesicle concentration × time) to vesicles in solution,[2] we have performed time-resolved (TR) reflectivity experiments in a constant solution flow mode using low-concentration vesicle solutions (5−10 μg/mL), where the characteristic time of membrane completion is in the range of hundred of minutes. Each reflectivity measurement in the q range of ∼0.2−1.5 nm^{-1} lasted 14 min, thus permitting the acquisition of multiple frames until the end of the POPC membrane formation. The chosen ionic strength (150 mM NaCl) corresponds to conditions that are known to lead to the formation of high-quality bilayers.[3] Experimental runs at each different vesicle concentration were repeated twice with different silicon substrates and independently prepared vesicle solutions, where good reproducibility was observed (Supporting Information Figure 1).

In Figure 2, the raw TR reflectivity data for the formation of a POPC membrane at a vesicle solution concentration of 5 μg/mL are presented. In the first hour of the process, the reflectivity curve moves slightly below the initial Fresnel curve, indicating the presence of an extended diffuse lower sld layer (hydrocarbon tails of the lipids belonging to unfused adsorbed vesicles). At t = 70 min, we observe the appearance of a reflectivity minimum at $q \approx 0.65$ nm^{-1}, whereas at longer times a curve corresponding to an almost complete lipid bilayer on the surface is measured. The TR measurements at twice the concentration (Figure 3) reveal exactly the same behavior at a roughly 2 times faster pace.

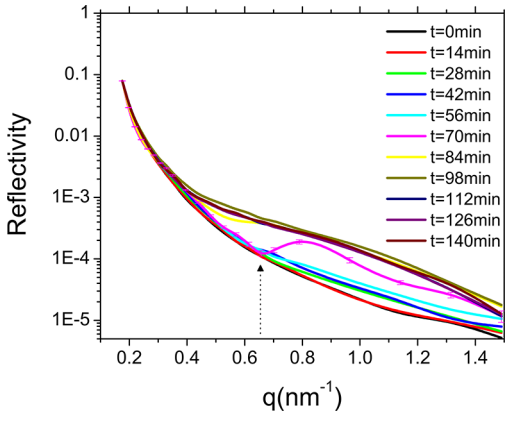

Figure 2. Raw reflectivity data during the formation of a POPC bilayer on SiO_2 via vesicle fusion. The solution concentration is 5 μg/mL. For the reflectivity curve measured at t = 70 min, error bars are depicted. The arrow indicates the position of the reflectivity minimum observed at t = 70 min.

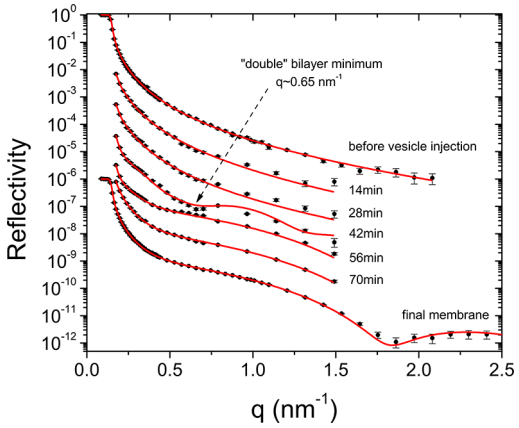

Figure 3. Neutron reflectivity measurements before, during, and after the formation of a POPC bilayer on SiO_2 via vesicle fusion. After the initial measurement, vesicles are injected into the measurement cell at a concentration of 10 μg/mL and reflectivity curves are acquired every 14 min in the q range of up to 1.5 nm^{-1}. The last curve at the bottom, represents a full measurement 4 h after the injection of the vesicles. Red curves represent model fits to the data. (See the text for details.) For clarity, successive curves are displaced by 1 order of magnitude.

Model fitting of the experimental curves (Figure 3) provides a detailed picture concerning the sld variation near the surface at different stages of the kinetic process (Figure 4). As expected, the initial reflectivity before the injection of the vesicle solution can be fitted by assuming only the existence of a thin (∼1.0 nm) and smooth (0.3 nm roughness) silicon oxide layer at the Si/D_2O interface. The next couple of curves can be fitted using a single diffuse extended layer on the surface, indicating the presence of adsorbed vesicles. Subsequently, in the intermediate stage (t = 42 min) data can be modeled only if we assume the existence of membrane patches partially covering the substrate (∼45%) and the additional existence of (a) a second sparse bilayer stack (∼12% coverage) on top of the first and (b) a diffuse and extended layer (adsorbed intact vesicles). Here we have to note that a single bilayer model characterized by high water penetration due to the existence of isolated bilayer patches or disordered membranes on the substrate could also present a minimum in the mentioned q range. However, no physically meaningful single-bilayer model can fit the reflectivity curves acquired at intermediate times (see also Supporting Information Figure 2). The final specular reflectivity curves can be fitted either using a single bilayer model close to full coverage (final state) or an additional diffuse layer that represents intact adsorbed vesicles (t = 56 min). The final POPC bilayer is characterized by an area per lipid equal to 0.61 nm^2 and by a hydrocarbon core thickness equal to 3.05 nm, both very close to the estimations in previous work.[25] (Refer to the Supporting Information for a table describing in detail all of the structural parameters.)

The partial formation of bilayer patches that is found by the fitting of the specular reflectivity data in the intermediate stage of membrane formation is also manifested as excess off-specular

DOI: 10.1021/acs.langmuir.7b02459
Langmuir 2017, 33, 10598−10605

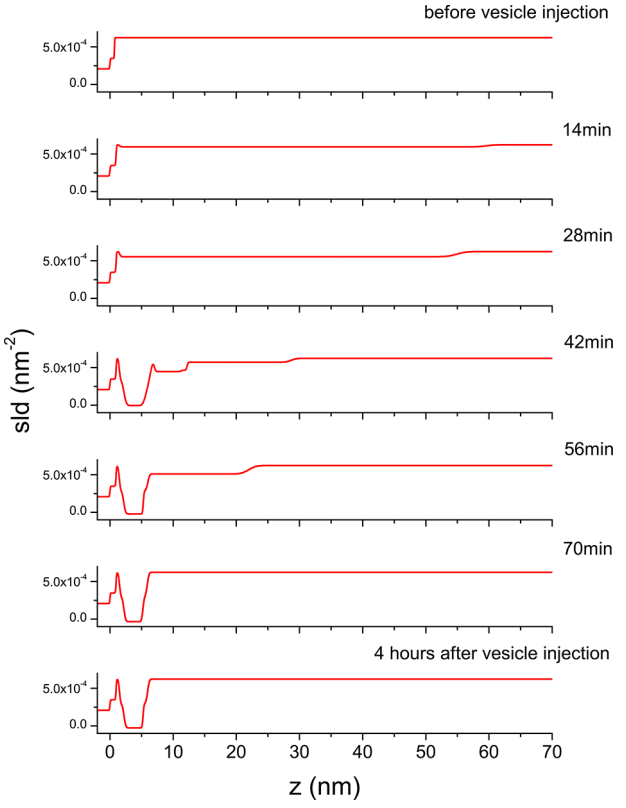

Figure 4. Scattering length density profiles before, during, and after the formation of a POPC bilayer on SiO_2 via vesicle fusion (solution concentration 10 μg/mL), as determined via the model fitting of the reflectivity data of Figure 3.

scattering in the plotted α_i vs a_f maps in Figure 5. We note that in the reflectivity maps before the adsorption of vesicles and in the final state where a complete membrane is formed, no appreciable scattering is present except along the specular reflectivity line. However, when reaching the intermediate stage, off-specular reflectivity (Yoneda wings) is observed running out of the critical edge, thus signifying a lateral inhomogeneity on the micrometer scale, parallel to the surface.[26] Here we relate this qualitative observation of diffuse scattering with the existence of membrane patches that partially cover the substrate and thus give rise to an apparent roughness that in turn induces the observed effect.

Further insight concerning the SLB formation can be obtained by calculating the overall amount of lipid adsorbed on the surface as a function of time based on the calculated sld profiles of Figure 4 using the equation $\Gamma = (M_{POPC}/N_A\nu_{POPC}) \int \phi_{POPC}(z)\, dz$, where N_A is Avogadro's number, ν_{POPC} = 1.25 nm^3 is the molecular volume in the liquid phase,[27] $M_{POPC} \approx$ 760.09 g/mol is the molecular weight, and $\phi_{POPC}(z)$ is the volume fraction profile of POPC molecules calculated from the sld profile. As seen in Figure 6, our results suggest an overshoot of the lipid mass on the substrate before reaching a single bilayer plateau in the final state. This effect is present in kinetic runs for all used lipid concentrations.

DISCUSSION

The general features of the TR reflectivity measurements are in agreement with the progressive adsorption of intact vesicles in the initial stage and subsequently their transformation to a complete single bilayer separated from the substrate by a thin water layer. However, the experimental observation of mass overshoot and more importantly of an early minimum in the reflectivity profile during the intermediate stage of the process needs further investigation. The position of the minimum ($q \approx$ 0.65 nm^{-1}) indicates the presence of partial double bilayer stacking ($\Delta = 2\pi/q$ = 9.7 nm $\simeq$ 2 times the bilayer thickness). The first possibility that comes to mind is related to the deformation and complete flattening of adsorbed vesicles under the influence of substrate attraction. In this respect, in this section we first treat theoretically the shape of an adsorbed vesicle on an attractive substrate, and then on the basis of the

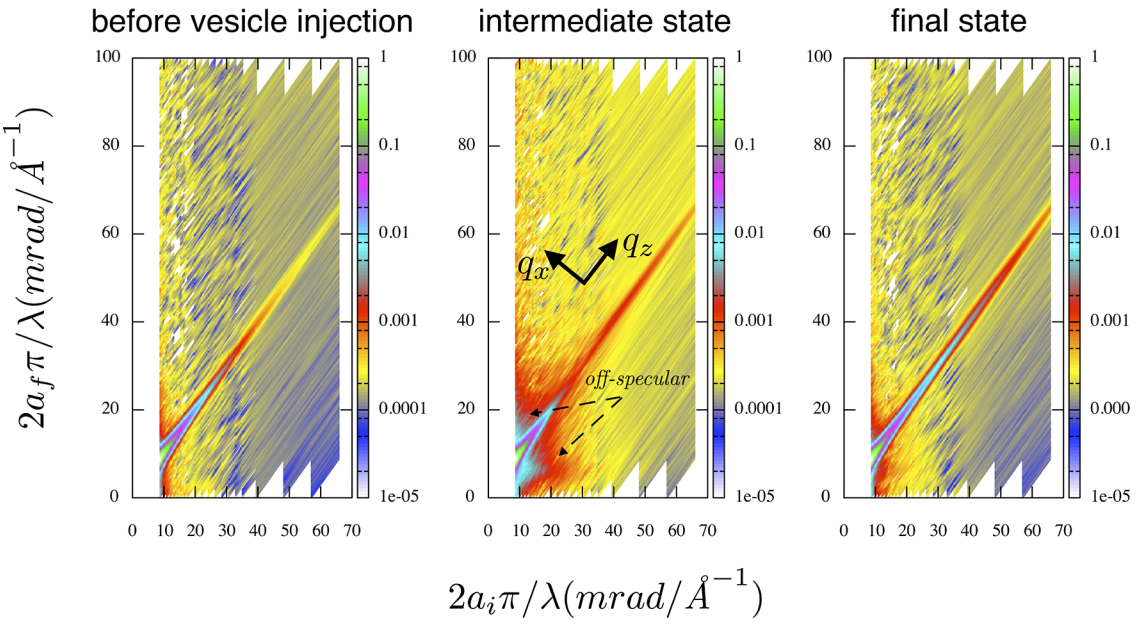

Figure 5. Off-specular and specular neutron reflectivity data during vesicle spreading. Note the appearance of off-specular scattering in the intermediate stage of vesicle formation, which indicates the existence of membrane patches on the Si surface.

DOI: 10.1021/acs.langmuir.7b02459
Langmuir 2017, 33, 10598−10605

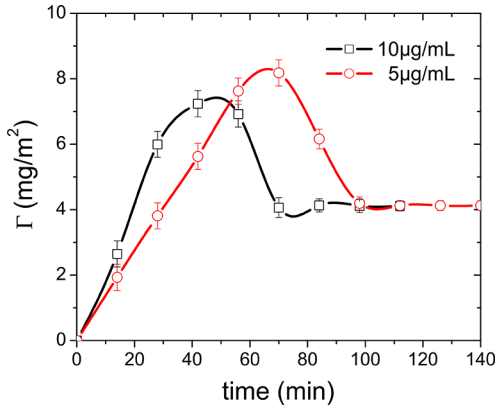

Figure 6. Evolution of the adsorbed lipid mass per unit area as a function of time (solution concentrations 5 and 10 μg/mL), as determined from the sld profiles of Figure 4. The curves passing through the data serve as a guide to the eye.

relevant conclusions, we discuss the implications of the present results for different possible vesicle spreading mechanisms.

Shape of Adsorbed Vesicles. Let us consider a lipid-bilayer vesicle with constant spherical topology and constant surface area S that adsorbs on a plane. (Note that as far as the steady state is considered, the lipid bilayer is permeable to water[28] so that the internal volume of the vesicle is not constant.) At equilibrium, for large enough vesicles allowing translational entropy loss to be neglected but small enough to neglect shape fluctuations, the free energy reduces to two terms:

$$E_{\text{free}} = \mathcal{E} + E_{\text{a}} \text{ with } \begin{cases} \mathcal{E} = \dfrac{k_{\text{c}}}{2}\displaystyle\int (c_1 + c_2)^2 \, \mathrm{d}S \\ E_{\text{a}} = -k_{\text{a}} \times a_{\text{fr}} S \end{cases} \tag{3}$$

Here, c_1 and c_2 are the local curvatures of the surface element $\mathrm{d}S$, k_{c} is the mean-curvature modulus of the bilayer, and $\mathcal{E}$ is the bending elastic potential (that increases as the shape deviates from the sphere). Also, E_{a} is the adhesion energy potential (that decreases for increasing area of the adhesion surface) with k_{a} being the adhesion constant and a_{fr} being the fraction of the adhering surface. The exact determination of which shape allows E_{free} to be minimized and how this shape depends on the vesicle size would involve the calculus of variations with Lagrange multipliers leading to a third- or fourth-order (depending on shape symmetry) nonlinear partial differential equation. This somewhat cumbersome method has already been used.[29] Instead, we used an alternative simplified strategy to approximate the result.

For reasons of symmetry, an adsorbed vesicle has a revolution z axis that is normal to the plane. Then, we make the following assumption: the lowest-energy surface of an adsorbed vesicle has a generatrix that is itself a lowest-energy curve. Note that this assumption is valid for the two limiting cases: spherical and completely flat vesicles. Thus, this approximation is expected to be reasonable for the intermediate cases.

Let us first deal with the "plane curves of minimal energy[30]" with constrained extremities and length.[31] Let us denote t as the parameter of the curve and $s(t) \in [0, L]$ as the curvilinear abscissa. The two extremities of the curve lie on the x axis and are distant from $2r$ (the radius of the adhering disk). We denote $\theta(s)$ as the angle formed by the tangent of the curve with the x axis (Figure 7). The curvature is $\theta' = \mathrm{d}\theta/\mathrm{d}s$, and the elastic

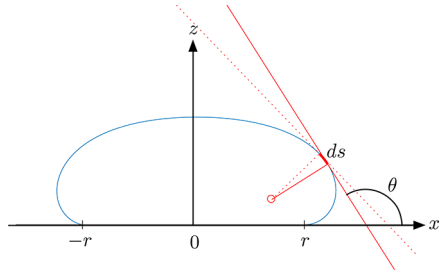

Figure 7. Plane curve of minimal energy for $L = 4r$.

energy that has to be minimized is $\int_0^L \theta'^2 \, \mathrm{d}s$. At any point (x, z), one has $\mathrm{d}x = \cos(\theta)\,\mathrm{d}s$ and $\mathrm{d}z = \sin(\theta)\,\mathrm{d}s$. Thus, the end-to-end vector of the curve is $\vec{v} = (\int_0^L \cos(\theta)\,\mathrm{d}s, \int_0^L \sin(\theta)\,\mathrm{d}s)$. It has been shown[30] that the curve of minimal energy we are looking for belongs to a set of spirals, which may be obtained from differential equations as

$$\theta' = \sqrt{a\cos(\theta) + b\sin(\theta) + c} \tag{4}$$

where a, b, and c are constants that have to be determined in order for the end-to-end vector to satisfy the constraint

$$\vec{v} = (-2r, 0) \tag{5}$$

In our case, to ensure the continuity of curvature at the extremities and the symmetry, we have

$$\theta(0) = 0,\ \theta(L) = 2\pi, \text{ and thus } \theta'(0) = \theta'(L) \tag{6}$$

Derivating eq 4 gives $2\theta'' = -a\sin(\theta) + b\cos(\theta)$. By integrating over the interval $[0, L]$ and using eqs 5 and 6, one obtains $b = 0$, and eq 4 reduces to

$$\theta' = \sqrt{a\cos(\theta) + c} \tag{7}$$

The lowest-energy shape of a vesicle of total area $S = 4\pi R^2$ was thus determined as follows.

For a given fraction a_{fr} of the adsorbed area, we can write the following:

1. The least-energy curve (generatrix of the non-adsorbed part) was determined by searching in eq 7 the couple (a,c) that minimizes $\|\vec{v} - (-2r, 0)\|$, with $r = (S_{\text{r}}/\pi \times a_{\text{fr}}/(1 - a_{\text{fr}}))^{1/2}$ and S_{r} being the area of the surface of revolution of the curve. This can be done by following the Nelder–Mead simplex method. Note that this step does not preserve the vesicle area S but only the length L. However, thanks to the invariance of the elastic energy of the surface under homothetic transformations (eq 8), the generatrix can be rescaled by a factor of $\sqrt{S/(S_{\text{r}} + \pi r^2)}$.
2. From the generatrix, the elastic energy of the surface is computed for a given a_{fr} value:

$$\mathcal{E}(a_{\text{f}}) = \frac{k_{\text{c}}}{2}\int_0^{L/2} (2K_{\text{m}})^2 \times 2\pi x \, \mathrm{d}s$$

$$\text{with } K_{\text{m}} = \frac{x(x''z' - x'z'') - z's'^2}{2xs'^3} \tag{8}$$

   where $'$ and $''$ denote first and second derivatives with respect to the curve parameter t.
3. Finally, the optimum value for a_{fr} that minimzes $E_{\text{free}}(a_{\text{fr}}) = \mathcal{E}(a_{\text{fr}}) - k_{\text{a}} \times a_{\text{fr}} S$ is numerically determined. This corresponds to the equilibrium shape.

DOI: 10.1021/acs.langmuir.7b02459
Langmuir 2017, 33, 10598−10605

Examples of shapes and size parameters relevant to the present experimental conditions are plotted in Figures 8 and 9. Note

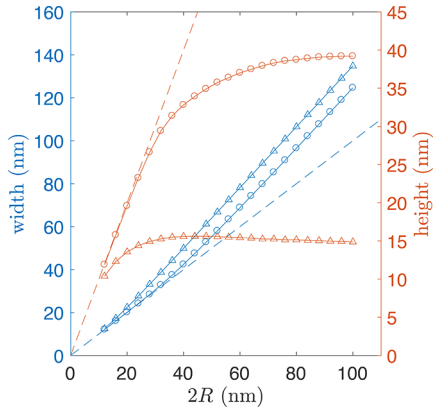

Figure 8. Equilibrium width and height of adsorbed vesicles versus initial vesicle radius R calculated for $k_a = 10^{-3}$ J m^{-2} and two values of k_c. (Left) Width (blue) and height (red) for $k_c = 1.5 \times 10^{-19}$ J (circles) and $k_c = 0.25 \times 10^{-19}$ J (triangles). Dashed lines have a slope of 1 corresponding to nondeformed spheres.

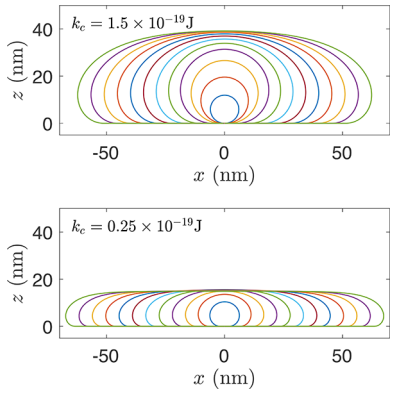

Figure 9. Adsorbed vesicle shapes for two values of k_c, corresponding to the data points of Figure 8.

that vesicle profiles of Figure 9 are similar to those already reported in ref 29 in the case of zero osmotic pressure and high stiffness, i.e., $\sqrt{k_c/k_a}$ larger than the thickness of the bilayer.

Implications for the Spreading Mechanism. In the present experiments, the values of the three parameters (R, k_a, k_c) that affect the shape of adsorbed vesicles can be estimated from the literature and from our initial vesicle characterization. A mean vesicle radius of $R \approx 52$ nm was estimated by DLS measurements. From previous experimental investigations,[32] we may find estimations of the POPC bending modulus in the liquid phase on the order of $k_c \approx 1.5 \times 10^{-19}$ J, although values of as low as 0.25×10^{-19} J have also been reported. Additionally, from the work of Anderson et al.[10] where the adhesion energy between silica and DMPC (a lipid with the same headgroup as POPC) was measured, we get $k_a \approx 1$ mJ/m^2. Using these values, we estimate the shape of POPC vesicles adsorbed on SiO_2 (Figure 9).

A simple inspection of the vesicle shapes reveals that for stiffer POPC membranes ($k_c \approx 1.5 \times 10^{-19}$ J, which is the value at which most experimental studies are converging) the energy gain due to the adhesion interaction of the vesicle headgroups with the substrate is not high enough to cause a severe deformation of the vesicle, and the vesicle height for $R > 25$ m is equal to about 40 nm. Considering the lowest reported k_c value and thus a "softer" vesicle, we find that the vesicle deforms much more but still the predicted membrane height of ~15 nm for $R > 15$ nm is larger than that of two stacked bilayers. This leads us to the conclusion that for the whole range of reported POPC k_c values, theory does not predict adsorbed vesicle conformations that may explain the observed characteristic reflectivity minimum (Figures 2 and 3) in the intermediate stage of membrane formation. It is interesting that even in the case where adsorbed vesicles on the substrate start to fuse with each other, thus leading to the formation of adsorbed vesicles with larger radii, the above conclusions are not affected because a plateau vesicle height is expected to be reached quite early as a function of vesicle size (Figure 8).

We can also think of two other possible sources for the observed bilayer stacking: (a) the presence of a high degree of oligolamellar vesicles in the sample and (b) the adsorption of incoming vesicles on top of already formed bilayer patches on the surface. The first scenario can be excluded by the findings of the cryo-TEM investigation. Concerning the second case, if vesicles had a propensity to simply adsorb on top of already formed membrane patches, such a state should have been easily detectable[33] from the fit of the full reflectivity curve after the end of the membrane formation. Instead, we can adequately fit the reflectivity results using only a three-layer model (heads/tails/heads) for a single POPC membrane on the silicon oxide surface.

Excluding complete vesicle flattening, vesicle adsorption on SLB, and also the existence of significant oligolamellarity in our sample as possible reasons for the observed partial bilayer

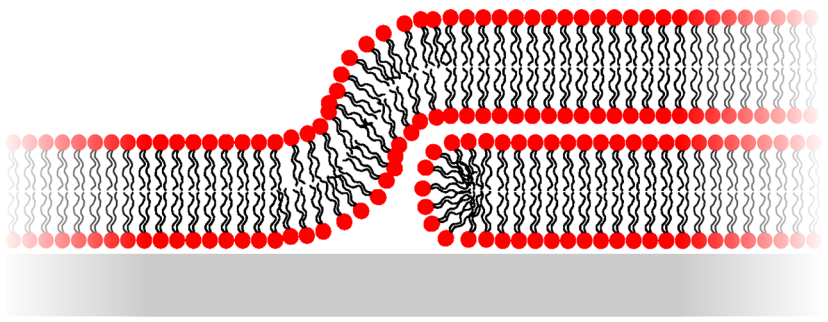

Figure 10. Schematic representation of the proposed arrangement of vesicles near bilayer edges in the intermediate stage of membrane formation. Such a molecular distribution corresponds to the observed characteristic double bilayer peak, observed in the measured reflectivity. Note that the lower right bilayer belongs to an adorbed membrane patch, whereas the "sigmoid" upper bilayer represents the lower part of an unfused vesicle.

DOI: 10.1021/acs.langmuir.7b02459
Langmuir 2017, 33, 10598−10605

stacking in the intermediate stage of membrane formation, we have to turn to other possible explanations of this effect. In the framework of proposed SLB formation mechanisms[8,14,15] where vesicles show an enhanced affinity for bilayer patch edges, after the initial adsorption of intact vesicles on the substrate and by reaching a critical vesicle surface density, fusion and/or rupture events produce bilayer patches that act as nucleation points that further attract neighboring vesicles. This process is catalyzed by the presence of thermodynamically unstable bilayer edges at the perimeter of the patches. Consenquently, in the intermediate stage of SLB formation the substrate is partially covered by lipid membranes with edges that are decorated by adsorbed intact vesicles. (See Figure 10 for a schematic visualization of the concept.) This transient state may produce a reflectivity curve such as the one observed during our TR reflectivity scans, thus adding further support for such an edge-catalyzed mechanism that was initially proposed on the basis of real-space microscopy techniques. We point out that other possible SLB formation pathways that involve a trapped thick water layer under ruptured vesicles can be used to explain the observed reflectivity; however, there is no reason that the separation from the substrate should be almost the same as the thickness of the POPC membrane.

Having attributed the observed bilayer stacking to the edge-catalyzed vesicle adsorption, we turn to the second interesting result of our study, i.e., the observed overshoot of the adsorbed mass during membrane formation (Figure 6), which looks quite similar to the measured frequency overshoot that is typically found in QCM experiments.[2,9] This frequency overshoot in relation to the energy dissipation of the QCM is usually interpreted as a release of trapped water by the vesicles during their rupture and after having reached a critical concentration at the surface. However, the analysis of our reflectivity results in accord with previous TR fluoresence microscopy investigations[14] suggest that there is indeed an excess of lipid mass on the substrate compared to the final mass of the single POPC bilayer, which means that after the intermediate stage of the membrane formation process there is a large uptake of lipids from the substrate.[4,16] The most straightforward explanation[15] is that intact vesicles at the edges of bilayer patches desorb because they do not experience attraction anymore as the patches start to coalesce.

In a previous TR X-ray reflectivity study of (1,2-dioleoyl-*sn*-glycero-3-phosphocholine) DOPC vesicle fusion of SiO_2[5] with quite similar solvent conditions except for the presence of divalent salts ($CaCl_2$), the authors did not report any similar effects (mass overshoot, bilayer stacking) but only the progressive coverage of the surface by growing bilayer patches. We can postulate that divalent cations Ca^{2+} may largely influence the vesicle−substrate and intravesicle interactions so that the overall spreading mechanism is affected. However, we would have expected the even weak (due to reduced contrast in X-ray experiments) detection of unfused vesicle layers in the initial stage after the exposure of the substrate to the vesicle solution. On the other hand, previous neutron reflectivity investigations[6] did not possess the time resolution required for the observation of distinct transient structural intermediates

CONCLUSIONS

We have followed the formation process of SLB on silicon oxide using TR reflectivity, thus obtaining a unique nanometer-scale picture of the near-surface molecular distribution as the membrane is formed. The main results of our work are related to the partial coverage of the surface by stacked bilayers at the intermediate stage of the process and also to the desorption of lipid vesicles as the SLB is reaching completion. An analysis of the data and theoretical arguments concerning the shape of adsorbed vesicles suggests that the most probable cause for this behavior comes from the conformation of newly recruited vesicles near the edges of membrane patches on the substrate, which are also forced to desorb in the later stage when bilayer patches are growing and merging, covering the whole surface. We argue that these observations add proof concerning the validity of the recently proposed SLB formation mechanism through edge-facilitated vesicle fusion.

ASSOCIATED CONTENT

Supporting Information

The Supporting Information is available free of charge on the ACS Publications website at DOI: 10.1021/acs.langmuir.7b02459.

Additional reflectivity data, fitting curves, and used model parameters (PDF)

AUTHOR INFORMATION

Corresponding Author

*E-mail: a.koutsioumpas@fz-juelich.de.

ORCID

Alexandros Koutsioubas: 0000-0001-9417-5108

Notes

The authors declare no competing financial interest.

ACKNOWLEDGMENTS

The authors thank Dr. Pierre Lairez for helpful mathematical insights concerning the calculation of adsorbed vesicle shape. Also, A.K. thanks Dr. Stefan Mattauch for illuminating discussions related to off-specular reflectivity.

REFERENCES

(1) Reviakine, I.; Brisson, A. Formation of Supported Phospholipid Bilayers from Unilamellar Vesicles Investigated by Atomic Force Microscopy. *Langmuir* **2000**, *16*, 1806−1815.

(2) Keller, C. A.; Glasmästar, K.; Zhdanov, V. P.; Kasemo, B. Formation of Supported Membranes from Vesicles. *Phys. Rev. Lett.* **2000**, *84*, 5443−5446.

(3) Cho, N.-J.; Frank, C. W.; Kasemo, B.; Hook, F. Quartz crystal microbalance with dissipation monitoring of supported lipid bilayers on various substrates. *Nat. Protoc.* **2010**, *5*, 1096−1106.

(4) Reimhult, E.; Zäch, M.; Höök, F.; Kasemo, B. A Multitechnique Study of Liposome Adsorption on Au and Lipid Bilayer Formation on SiO2. *Langmuir* **2006**, *22*, 3313−3319.

(5) Wang, S. T.; Fukuto, M.; Yang, L. *In situ* x-ray reflectivity studies on the formation of substrate-supported phospholipid bilayers and monolayers. *Phys. Rev. E* **2008**, *77*, 031909.

(6) Gutberlet, T.; Klösgen, B.; Krastev, R.; Steitz, R. Neutron Reflectivity as Method to Study in-Situ Adsorption of Phospholipid Layers to Solid-Liquid Interfaces. *Adv. Eng. Mater.* **2004**, *6*, 832−836.

(7) Brian, A. A.; McConnell, H. M. Allogeneic stimulation of cytotoxic T cells by supported planar membranes. *Proc. Natl. Acad. Sci. U. S. A.* **1984**, *81*, 6159−6163.

(8) Richter, R. P.; Bérat, R.; Brisson, A. R. Formation of Solid-Supported Lipid Bilayers: An Integrated View. *Langmuir* **2006**, *22*, 3497−3505.

(9) Lind, T. K.; Cardenas, M. Understanding the formation of supported lipid bilayers via vesicle fusion-A case that exemplifies the need for the complementary method approach (Review). *Biointerphases* **2016**, *11*, 020801.

DOI: 10.1021/acs.langmuir.7b02459
Langmuir 2017, 33, 10598−10605

(10) Anderson, T. H.; Min, Y.; Weirich, K. L.; Zeng, H.; Fygenson, D.; Israelachvili, J. N. Formation of Supported Bilayers on Silica Substrates. *Langmuir* **2009**, *25*, 6997−7005.
(11) Richter, R. P.; Brisson, A. R. Following the Formation of Supported Lipid Bilayers on Mica: A Study Combining AFM, QCM-D, and Ellipsometry. *Biophys. J.* **2005**, *88*, 3422−3433.
(12) Cremer, P. S.; Boxer, S. G. Formation and Spreading of Lipid Bilayers on Planar Glass Supports. *J. Phys. Chem. B* **1999**, *103*, 2554−2559.
(13) Akesson, A.; Lind, T.; Ehrlich, N.; Stamou, D.; Wacklin, H.; Cardenas, M. Composition and structure of mixed phospholipid supported bilayers formed by POPC and DPPC. *Soft Matter* **2012**, *8*, 5658−5665.
(14) Weirich, K. L.; Israelachvili, J. N.; Fygenson, D. K. Bilayer Edges Catalyze Supported Lipid Bilayer Formation. *Biophys. J.* **2010**, *98*, 85−92.
(15) Plunkett, P.; Camley, B. A.; Weirich, K. L.; Israelachvili, J.; Atzberger, P. J. Simulation of edge facilitated adsorption and critical concentration induced rupture of vesicles at a surface. *Soft Matter* **2013**, *9*, 8420−8427.
(16) Reimhult, E.; Larsson, C.; Kasemo, B.; Höök, F. Simultaneous Surface Plasmon Resonance and Quartz Crystal Microbalance with Dissipation Monitoring Measurements of Biomolecular Adsorption Events Involving Structural Transformations and Variations in Coupled Water. *Anal. Chem.* **2004**, *76*, 7211−7220.
(17) Andrecka, J.; Spillane, K. M.; Ortega-Arroyo, J.; Kukura, P. Direct Observation and Control of Supported Lipid Bilayer Formation with Interferometric Scattering Microscopy. *ACS Nano* **2013**, *7*, 10662−10670.
(18) Koutsioubas, A. Combined Coarse-Grained Molecular Dynamics and Neutron Reflectivity Characterization of Supported Lipid Membranes. *J. Phys. Chem. B* **2016**, *120*, 11474−11483.
(19) Schneider, C. A.; Rasband, W. S.; Eliceiri, K. W. NIH Image to ImageJ: 25 years of image analysis. *Nat. Methods* **2012**, *9*, 671−675.
(20) Mattauch, S.; Koutsioubas, A.; Putter, S. MARIA: Magnetic Reflectometer with high Incident Angle. *Journal of large-scale research facilities* **2015**, *1*, A8.
(21) Jaksch, S.; Lipfert, F.; Koutsioubas, A.; Mattauch, S.; Holderer, O.; Ivanova, O.; Frielinghaus, H.; Hertrich, S.; Fischer, S. F.; Nickel, B. Influence of Ibuprofen on Phospholipid Membranes. *Phys. Rev. E* **2015**, *91*, 022716.
(22) Abelès, F. La Théorie Générale des Couches Minces. *J. Phys. Radium* **1950**, *11*, 307−309.
(23) Névot, L.; Croce, P. Caractérisation des Surfaces par Réflexion Rasante de Rayons X. Application á l'Étude du Polissage de Quelques Verres Silicates. *Rev. Phys. Appl.* **1980**, *15*, 761−779.
(24) Ott, F.; Kozhevnikov, S. Off-specular data representations in neutron reflectivity. *J. Appl. Crystallogr.* **2011**, *44*, 359−369.
(25) Kucerka, N.; Nieh, M.-P.; Katsaras, J. Fluid phase lipid areas and bilayer thicknesses of commonly used phosphatidylcholines as a function of temperature. *Biochim. Biophys. Acta, Biomembr.* **2011**, *1808*, 2761−2771.
(26) Paul, N.; Paul, A.; Mattauch, S.; Muller-Buschbaum, P.; Boni, P.; Lux-Steiner, M. C. Interfacial smoothening of polymer multilayers with molecules: a new approach in growing supramolecular layer structures. *Soft Matter* **2013**, *9*, 10117−10128.
(27) Pandit, S. A.; Chiu, S.-W.; Jakobsson, E.; Grama, A.; Scott, H. Cholesterol Surrogates: A Comparison of Cholesterol and 16:0 Ceramide in {POPC} Bilayers. *Biophys. J.* **2007**, *92*, 920−927.
(28) Mathai, J. C.; Tristram-Nagle, S.; Nagle, J. F.; Zeidel, M. L. Structural Determinants of Water Permeability through the Lipid Membrane. *J. Gen. Physiol.* **2008**, *131*, 69−76.
(29) Seifert, U.; Lipowsky, R. Adhesion of vesicles. *Phys. Rev. A: At., Mol., Opt. Phys.* **1990**, *42*, 4768−4771.
(30) Horn, B. K. P. The Curve of Least Energy. *ACM Trans. Math. Softw.* **1983**, *9*, 441−460.
(31) Kallay, M. Plane Curves of Minimal Energy. *ACM Trans. Math. Softw.* **1986**, *12*, 219−222.
(32) Dimova, R. Recent developments in the field of bending rigidity measurements on membranes. *Adv. Colloid Interface Sci.* **2014**, *208*, 225−234. Special issue in honour of Wolfgang Helfrich.
(33) Lind, T. K.; Cardenas, M.; Wacklin, H. P. Formation of Supported Lipid Bilayers by Vesicle Fusion: Effect of Deposition Temperature. *Langmuir* **2014**, *30*, 7259−7263.

DOI: 10.1021/acs.langmuir.7b02459
Langmuir 2017, 33, 10598−10605